A NOVEL METHOD FOR 3D PROSTATE MR-HISTOLOGY REGISTRATION USING ANATOMICAL LANDMARKS

Cecilia Hughes[1,2,3]*, Olivier Rouviere*[3,4]*, Florence Mege-Lechevallier*[5]*, Remi Souchon*[3] *and Remy Prost*[2]

[1]CCITI, 14 rue Jean Giono, 21000 Dijon, France
[2]Université de Lyon, CREATIS; CNRS UMR5220; Inserm U1044; INSA-Lyon; Université Lyon 1, France
[3]Inserm, U1032, LabTau, 69003 Lyon, France; Université de Lyon, 69003 Lyon, France
[4]Hospices Civils de Lyon, Dept. Urinary and Vascular Radiology, Hôpital Edouard Herriot, Lyon, France
[5]Hospices Civils de Lyon, Dept. Histopathology, Hôpital Edouard Herriot, Lyon, France
e-mail: cecilia.hughes@inserm.fr

ABSTRACT

No current imaging technique is capable of detecting with precision tumours within the prostate. To evaluate each technique, the histology data must be registered to the imaged data. As the histology slices cannot be assumed to be cut along the same plane as the imaged data was acquired, the registration must be considered as a 3D problem. We propose a novel 3D registration method which uses the ejaculatory ducts, an anatomical landmark present in every prostate and visible in both MR and histology. The method has been tested on 3 prostate specimens. The aligned histology slices are first shear corrected, with an average angular error after correction of $2.83 \pm 1.46°$. The MR-histology registration accuracy, evaluated operator-independently, is on average 1.50 ± 0.74 mm.

Index Terms— Histology, MRI, Prostate, Registration

1. INTRODUCTION

Prostate cancer is the most common malignancy among men and the third highest cause of mortality in Europe in 2008 [1]. Imaging is important in the diagnosis, local staging and treatment follow-up and is a powerful tool as most imaging techniques are non-invasive, non-destructive and can provide dynamic real-time data and repeated measurements [2]. Each technique has advantages, disadvantages and specific indications, yet no current imaging method is capable of detecting with precision tumours within the gland and no consensus exists regarding the use of imaging techniques [2].

The critical issue in prostate cancer is distinguishing between benign and malignant tissue with the ground truth information contained in the histology slices of the prostatectomy specimen. To evaluate each imaging technique and determine the optimum combination of techniques, the histology data must be precisely mapped to the imaged data. For each imaging technique, a quantitative analysis of the signal in the zones corresponding exactly to the histology tumours would enable a definition of the signal characteristics of prostate cancerous tissue for that technique.

Currently, for the diagnosis and localisation of prostate cancer, the most effective imaging method is MR, provided it is multi-parametric, i.e. it combines different sequences (e.g. T_2-weighted imaging, diffusion-weighted imaging, dynamic contrast-enhanced imaging and/or spectroscopy) [3].

MR-histology registration is a challenging problem, due in particular to (i) the complex deformation and tissue loss caused by the extraction of the prostate from the body and the histology sectioning process and (ii) the significant differences in the two image modalities, specifically the difference in resolution, mm for MR and µm for histology, means that features clearly visible in histology may not be detectable in MR.

There are two general approaches to register the histology data to the *in vivo* pre-operative images; the first is a 2D-2D registration, which assumes that the prostate specimen is sliced along the same plane orientation as the *in vivo* images were acquired. Various methods have been proposed to ensure the orientation is held constant for imaging and slicing [4], however no consensus exists as to an optimum technique. In general, it cannot be assumed that the histology slices are cut along the same plane as the imaged data was acquired and so the mapping must be considered as a 3D problem. Hence the second approach is a 3D registration of the imaged data volume with the histology volume.

Various methods have been proposed in the literature to achieve this 3D registration, [5] manually segments the prostate in both modalities and then optimises the superposition of the two point clouds. The method described in [6] also uses the prostate boundary, as well as internal landmarks, to guide the registration. Due to the aforementioned deformation and tissue loss, we do not consider the prostate boundary to be a reliable feature to guide the registration. Other methods propose breaking the registration

into sub-registration tasks involving intermediate modalities, often block-face images acquired during the histology sectioning process [7]. However the acquisition of such images lengthens the processing time of the clinical routine. The registration methods presented in [8,9] were developed using images of the brain, an organ with far greater structural detail, and thus information redundancy, than the prostate. The method detailed in [10] first estimates, in a 2D-2D sense, the histology-MR slice correspondences, then determines the 3D registration between the histology and MR volumes. However the authors noted that the 3D registration caused only a small change to the slice correspondences.

We propose and describe here a novel method for 3D prostate MR-histology registration. The histology slices are first aligned using the method described in [11] whereby three fiducial needles are inserted into the fresh prostate specimen. We detail here a method to correct for the shear error that may be present in the aligned histology slices, thus ensuring that we have an accurately reconstructed histology volume. The 3D MR-histology registration is then achieved using the ejaculatory ducts, an anatomical landmark present in every prostate specimen, and visible in both histology and MR images acquired in standard clinical routine. Before fixation and histology sectioning, an *ex vivo* MR acquisition of the fresh prostate specimen, with the fiducial needles inserted, is performed. These needles, visible in both histology and MR *ex vivo*, enable us to report a quantitative and operator-independent evaluation of the accuracy of the proposed registration method, before applying it to *in vivo* MR data.

2. METHOD

Candidate patients were those, at our institution, that had undergone an *in vivo* MR prostate examination and for whom a radical prostatectomy was planned. Following the operation, three catheter needles with rigid plastic sheaths were inserted, each at a unique angle, into the fresh prostate specimen, using the apparatus described in [11], see figure 1. The needles were then removed, leaving the sheaths in place and a MR acquisition of the specimen was performed, T_2-weighted spin echo sequence, 3T clinical scanner (GE Healthcare, USA), voxel size 0.31x0.31x2mm, TE/TR = 116ms/4250ms. After formaldehyde fixation, the sheaths were removed and the prostate sectioned, from the apex to the base, into 6 mm sections. The paraffin-embedded sections are sliced using a microtome (slice thickness 4 µm, inter-spacing 1000 µm) and the whole-mount slices are digitised and rigidly aligned, as detailed in [11], see figure 2a.

2.1. Histology Shear Correction

The sectioning of the specimen causes the 3D conformation of the organ to be lost and it cannot be recovered in the absence of external information, a problem referred to as the 'banana problem' [8] or the 'z-shift effect' [9]. A shear correction is thus necessary for the histology slices aligned using the method described in [11].

In order to measure the model geometry of the three fiducial needles, and thus to have the 'external information' required, a rectangular sample of 3% agar was prepared. Needles were inserted using the apparatus [11], see figure 1, and a MR acquisition of the sample was acquired. The fiducial markers, created by the needles, and visible in the MR axial images, were detected. Three least-squares 3D lines passing through the markers were calculated, the model needles. The three model needles were arbitrarily labelled as model needle 1, 2 and 3. For each needle, the direction vector $\vec{AB}_n, n \in \{1,2,3\}$ was calculated, describing the direction at which the needle is inserted. As the apparatus guides the insertion of the needles into the prostate from the apex to the base of the prostate, the vectors $\vec{AB}_n$, are the model direction vectors of the needles from the apex to the base, see figure 1.

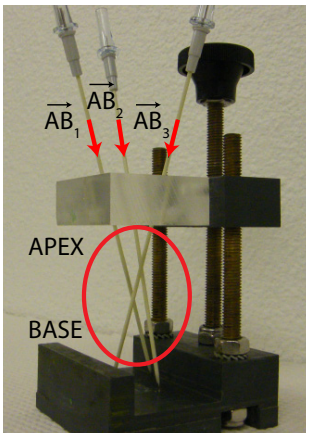

Fig. 1. Apparatus to guide the insertion of 3 needles into a prostate specimen from the apex to the base. $\vec{AB}_n, n \in \{1,2,3\}$ denote the direction vectors of the three needles.

The histology slices of each patient dataset had been aligned, from the apex to the base, using the method described in [11], see figure 2a. It is undetermined at this point the correspondence between the three needles in the patient dataset and the three model needles. It should be noted that though care was taken when the histology slices were digitsed that the normal vector of each slice was oriented in the same direction, i.e. that no 'flip orientation' between the slices need be taken into account, the ensemble of histology slices may need to be flipped.

In order to determine the correspondence between the three needles in the patient dataset and the three model needles, the 3! possible permutations are generated and each is tested with and without a flip applied to the ensemble of histology slices in the patient dataset, thus a total of 12 permutations, $p \in \{1,2,...,12\}$. To test each permutation,

first, the needles in the patient dataset are labelled (as needle 1, 2 and 3) according to the permutation under test and the least-squares rigid affine transform (rotation R and translation t) [12] is calculated in order to align the three markers at the apex patient histology slice with the three markers at the apex of the agar model. The transformation is applied to the ensemble of histology slices in the patient dataset. The error of the alignment $E_1(p)$ is defined as the mean of the distances between the corresponding markers at the apex of the agar model and the transformed apex patient histology slice. The direction vector of each of the three needles in the patient dataset is then calculated, denoted as $\vec{AB}_{p,n}$ and the parameters α, β of the shear matrix T, defined as

$$T = \begin{bmatrix} 1 & 0 & \alpha \\ 0 & 1 & \beta \\ 0 & 0 & 1 \end{bmatrix} \tag{1}$$

are calculated by minimising the function $E_2(p)$ defined as

$$E_2(p) = \sqrt{\sum_{n=1}^{3} \cos^{-1}\left(\frac{\langle \vec{AB}_n, T(\vec{AB}_{p,n})\rangle}{\|\vec{AB}_n\|\|T(\vec{AB}_{p,n})\|}\right)} \tag{2}$$

where $\langle f, g\rangle$ indicates the dot product of vector f and g. The error of each permutation is defined as the average of $E_1(p)$ and $E_2(p)$. The permutation with the minimum error indicates

- if the ensemble of patient histology slices need to be flipped
- the correspondence between the three needles in the patient dataset and the three model needles
- the parameters α and β of the optimal shear matrix T to be applied to the patient histology slices in order to recover the 3D conformation of the organ

2.2. MR – Histology Registration

To 3D register the prostate histology slices with the MR data, we have developed a method based on the use of the ejaculatory ducts. The ejaculatory ducts are paired structures, referred to here as the left and right ejaculatory duct, which begin at the seminal vesicles, pass through the prostate gland along a curved path and enter into the urethra. They are an anatomical landmark present in every prostate and are visible in both MR and histology. They have an average luminal diameter of 1.7 ± 0.3 mm in the proximal section, 0.6 ± 0.1 mm in the middle section and 0.3 ± 0.1 mm in the distal section [13].

2.2.1. Identification of the ejaculatory ducts

The MR axial images are visualised using OsiriX software (OsiriX Foundation, Switzerland). A point is placed at each location that the left or right ejaculatory duct is visible. The 3D coordinates of these points are exported and read into MATLAB (The Mathworks, USA). The aligned, shear corrected histology slices are visualised using MATLAB. The boundaries of the left and right ejaculatory ducts are outlined in the images in which they are visible and the centre of gravity of the outline is calculated. The resulting vector of 3D coordinates for each ejaculatory duct in each imaging modality is referred to as the data points for that duct in that modality, and denoted as $\mathbf{v} = [\mathbf{v}_x, \mathbf{v}_y, \mathbf{v}_z]$, with N the number of coordinates in the vector.

2.2.2. 3D parametric curve fit

Each ejaculatory duct is represented by a 3D, 2nd order parametric curve $\mathbf{f}(t)$ given by

$$\mathbf{f}(t) = \begin{bmatrix} x(t) & y(t) & z(t) \end{bmatrix}, 0 \le t \le 1$$
$$\text{where } \begin{cases} x(t) = c_{x,1}t^2 + c_{x,2}t + c_{x,3} \\ y(t) = c_{y,1}t^2 + c_{y,2}t + c_{y,3} \\ z(t) = c_{z,1}t^2 + c_{z,2}t + c_{z,3} \end{cases} \tag{3}$$

For each dimension $d, d \in \{x, y, z\}$ the polynomial coefficients $(c_{d,1}, c_{d,2}, c_{d,3})$ are independently calculated in a least-squares sense from the matrix

$$\begin{bmatrix} \mathbf{t}^2 & \mathbf{t}^1 & \mathbf{t}^0 \end{bmatrix} \begin{bmatrix} c_{d,1} \\ c_{d,2} \\ c_{d,3} \end{bmatrix} = \mathbf{v}_d \tag{4}$$

where $\mathbf{v}_d$ indicates the vector of data points in the dimension $d \in \{x, y, z\}$ of the manually detected duct and $\mathbf{t}^2, \mathbf{t}^1, \mathbf{t}^0$ the vectors of the powers of the parameter t with

$$\left\{\mathbf{t}^k\right\}_i = \left(\frac{i}{N-1}\right)^k, i = 0, ..., N-1 \tag{5}$$

where N is the number of coordinates in the data point vector.

From the 3×3 polynomial coefficient matrix $\mathbf{c}$, $\{\mathbf{c}\}_{d,j} = c_{d,j}$ with $d \in \{x, y, z\}$ and $j \in \{1, 2, 3\}$, the curve is reduced to a vector of points in 3D space, $\mathbf{p}$, such that the distance along the curve between two points, $\|p_\gamma, p_{\gamma+1}\| = \Delta$. We denote the vectors as $\mathbf{p}_R^H$ and $\mathbf{p}_L^H$ for the histology right and left ejaculatory ducts respectively, and similarly $\mathbf{p}_R^M$ and $\mathbf{p}_L^M$ for the MR ejaculatory ducts.

2.2.3. Registration of the curves

The MR-histology registration problem has been reduced to the registration of two vectors of equally spaced points ($\mathbf{p}_R^M$ and $\mathbf{p}_L^M$) with two other vectors of equally spaced points ($\mathbf{p}_R^H$ and $\mathbf{p}_L^H$). The registration transformation is calculated such as to align the MR vectors with the histology vectors; we thus refer to the MR vectors as the *moving set* and the histology vectors as the *static set*. Note that the point correspondence between the static and moving sets is unknown.

Considering first the right ejaculatory duct, we denote the number of points in the histology vector, $\mathbf{p}_R^H$ as $|\mathbf{p}_R^H|$ and the number of points in the MR vector $\mathbf{p}_R^M$ as $|\mathbf{p}_R^M|$. If $|\mathbf{p}_R^H| < |\mathbf{p}_R^M|$, we determine each possible subset of points of length $|\mathbf{p}_R^H|$ from the vector $\mathbf{p}_R^M$, respecting the relative order of the points. Similarly, if $|\mathbf{p}_R^H| > |\mathbf{p}_R^M|$, we determine each possible subset of points of length $|\mathbf{p}_R^M|$ from $\mathbf{p}_R^H$. For either case, we denote the number of possible subsets as N_R. The left ejaculatory duct is considered in the same manner, with the number of possible subsets denoted as N_L.

We iterate through each possible subset, calculating for each iteration the affine rigid registration (rotation, translation) using Procrustes analysis, see pseudo-code below. The registration error for each iteration is defined as the average distance between the corresponding points of the static and moving set after the registration has been applied. The minimum error indicates the subsets of the longer left and right ejaculatory ducts that correspond to the shorter left and right ejaculatory ducts and the transformation matrix to align them.

Pseudo-code

Assuming that $|\mathbf{p}_R^H| < |\mathbf{p}_R^M|$ and $|\mathbf{p}_L^H| < |\mathbf{p}_L^M|$
for $i = 1 \rightarrow N_R$ **do**
  histo right ejac. duct $\leftarrow \mathbf{p}_R^H$
  MR right ejac. duct $\leftarrow$ subset i of $\mathbf{p}_R^M$
  for $j = 1 \rightarrow N_L$ **do**
    histo left ejac. duct $\leftarrow \mathbf{p}_L^H$
    MR left ejac. duct $\leftarrow$ subset j of $\mathbf{p}_L^M$
    register [MR right ejac. duct, MR left ejac. duct]
      to [histo right ejac. duct, histo left ejac. duct]
    evaluate registration error $E(i, j)$
  end for
end for

3. RESULTS

Three prostate specimens were included in this study, with an average of 20 histology slices digitised per specimen (minimum 19, maximum 21) with an average pixel resolution of 0.03 mm. There were on average 16.3 MR axial images of the *ex vivo* specimen with a pixel resolution of 0.31 mm.

3.1. Histology Shear Correction

The angles of the model needles, from the apex to the base, with respect to the vertical, were measured from the MR acquisition of the agar sample. After alignment of the histology slices [11], but before the shear correction was applied, the average absolute difference between the angles of the patient dataset needles (from the apex to the base, with respect to the vertical) compared to the model needle angles was on average $9.32 \pm 6.27°$. After application of the shear correction, the average absolute difference in the angles was $2.83 \pm 1.46°$. Figure 2 shows the aligned histology slices of a sample patient dataset before and after the shear correction has been applied.

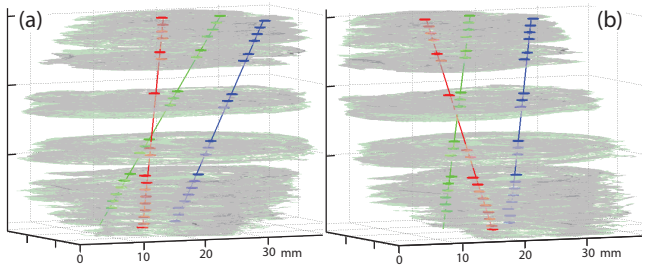

Fig. 2. Aligned histology slices of a sample patient dataset, (a) before and (b) after the shear correction has been applied. It can be visually appreciated that after shear correction, the angles of the needles in the patient dataset approach those of the model geometry (figure 1).

3.2. MR – Histology Registration

The right and left ejaculatory ducts were detected, on average, in 8 histology images and 4 MR images. After MR-histology registration, the average distance between the corresponding needles in the two modalities was 1.50 ± 0.74 mm. Figure 3 shows the two curved histology and MR ejaculatory ducts, which were used to guide the registration and the three needles which were used to quantify the quality of the registration.

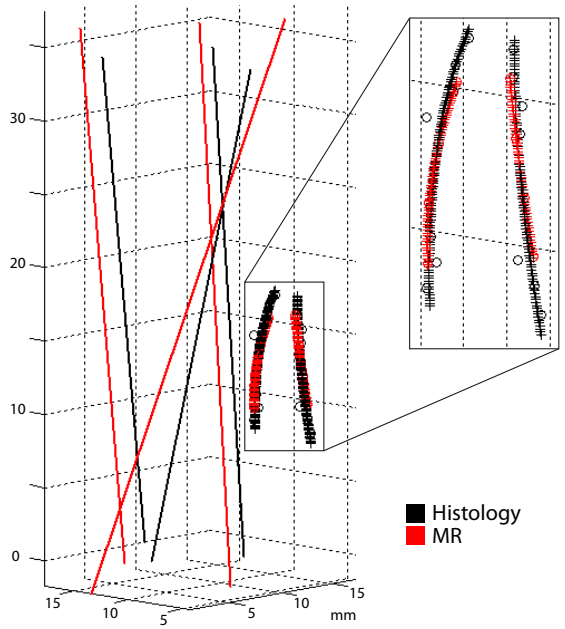

Fig. 3. 3D MR-histology registration achieved using the ejaculatory ducts, note the three fiducial needles and ejaculatory ducts in each modality. The data points, indicated by circles, are visible in the zoom of the ejaculatory ducts.

4. CONCLUSION

The angles of the model needles were measured from the MR acquisition of the agar sample. For each dataset of aligned histology slices, after the shear correction has been applied, the angles of the three needles should be equal to the model needle angles. Our method achieved an average absolute difference of $2.83 \pm 1.46°$. It should be noted that, unlike the agar, into which the needles were easily inserted, for a fresh prostate, due to its semi-solid consistency, a certain force is required to puncture the surface. This causes an unavoidable displacement of the prostate, repeated by the insertion of each proceeding needle. The result is that the exact geometry of the three needles is slightly different for each specimen and never exactly equal to the model geometry.

The ejaculatory ducts are an anatomical landmark that exist in every prostate specimen and are visible in both histology and MR. They thus provide a systematic means of registering the MR and histology data. The fact that they exist as paired structures, reduces the chance of their erroneous detection. The average registration error achieved, 1.50 ± 0.74 mm, is promising, considering that a cancer of volume $<$0.5 cm^3 is classified as clinically insignificant. We envisage further optimising the method and developing the database of prostate specimens on which it has been tested. The automatic detection of the ejaculatory ducts in both MR and histology should be examined. An attractive feature of the registration method is the time required, $<$5 sec per prostate specimen.

The next step is to use this method for 3D histology - MR *in vivo* registration. Though the MR *in vivo* resolution may be lower than the MR *ex vivo*, the fluid within the *in vivo* ejaculatory ducts improves their contrast, and thus a similar registration quality is hoped to be achieved. The overall goal being, that once the histology data is accurately registered to the MR *in vivo* data, the signal characteristics of cancerous tissue can be defined for each MR modality.

5. ACKNOWLEDGMENTS

This work was supported by an ANRT-CIFRE contract with CCITI, France.

6. REFERENCES

[1] J. Ferlay, D. M. Parkin, and E. Steliarova-Foucher, "Estimates of cancer incidence and mortality in europe in 2008." *Eur J Cancer*, vol. 46, no. 4, pp. 765–781, 2010.

[2] G. J. Kelloff, P. Choyke, D. S. Coffey, and P. C. I. W. G. , "Challenges in clinical prostate cancer: role of imaging." *AJR Am J Roentgenol*, vol. 192, no. 6, pp. 1455–1470, 2009.

[3] H. U. Ahmed, A. Kirkham, M. Arya, R. Illing, A. Freeman, C. Allen, and M. Emberton, "Is it time to consider a role for MRI before prostate biopsy?" *Nat Rev Clin Oncol*, vol. 6, no. 4, pp. 197–206, 2009.

[4] L. H. Chen, H. Ho, R. Lazaro, C. H. Thng, J. Yuen, W. S. Ng, and C. Cheng, "Optimum slicing of radical prostatectomy specimens for correlation between histopathology and medical images." *Int J Comput Assist Radiol Surg*, vol. 5, no. 5, pp. 471–487, 2010.

[5] L. S. Taylor, B. C. Porter, G. Nadasdy, P. A. di Sant'Agnese, D. Pasternack, Z. Wu, R. B. Baggs, D. J. Rubens, and K. J. Parker, "Three-dimensional registration of prostate images from histology and ultrasound." *Ultrasound Med Biol*, vol. 30, no. 2, pp. 161–168, 2004.

[6] Y. Ou, D. Shen, M. Feldman, J. Tomaszewski, and C. Davatzikos, "Non-rigid registration between histological and MR images of the prostate: A joint segmentation and registration framework," in *Proc. IEEE CVPR Workshops 2009*, 2009, pp. 125–132.

[7] H. Park, M. R. Piert, A. Khan, R. Shah, H. Hussain, J. Siddiqui, T. L. Chenevert, and C. R. Meyer, "Registration methodology for histological sections and *in vivo* imaging of human prostate." *Acad Radiol*, vol. 15, no. 8, pp. 1027–1039, 2008.

[8] G. Malandain, E. Bardinet, K. Nelissen, and W. Vanduffel, "Fusion of autoradiographs with an MR volume using 2-D and 3-D linear transformations." *Neuroimage*, vol. 23, no. 1, pp. 111–127, 2004.

[9] P. Yushkevich, B. Avants, L. Ng, M. Hawrylycz, P. Burstein, H. Zhang, and J. Gee, "3D mouse brain reconstruction from histology using a coarse-to-fine approach," in *Biomedical Image Registration*, 2006, vol. 4057, pp. 230–237.

[10] G. Xiao, B. N. Bloch, J. Chappelow, E. M. Genega, N. M. Rofsky, R. E. Lenkinski, J. Tomaszewski, M. D. Feldman, M. Rosen, and A. Madabhushi, "Determining histology-MRI slice correspondences for defining MRI-based disease signatures of prostate cancer." *Comput Med Imaging Graph*, vol. 35, no. 7-8, pp. 568–578, 2011.

[11] C. Hughes, O. Rouviere, F. Mege-Lechevallier, R. Souchon, and R. Prost, "Robust alignment of prostate histology slices with quantified accuracy," in *Proceedings SPIE*, 2012, p. 83141N.

[12] K. S. Arun, T. S. Huang, and S. D. Blostein, "Least-squares fitting of two 3-D point sets," *IEEE Transactions on Pattern Analysis and Machine Intelligence*, no. 5, pp. 698–700, 1987.

[13] H. T. Nguyen, J. Etzell, and P. J. Turek, "Normal human ejaculatory duct anatomy: a study of cadaveric and surgical specimens." *J Urol*, vol. 155, no. 5, pp. 1639–1642, 1996.